Title
PORE DRAB IN ALUMINA

Authors
Rodel, J.
Glaeser, A.M.

Publication Date
1988-10-01

Lawrence Berkeley Laboratory
UNIVERSITY OF CALIFORNIA

Materials & Chemical Sciences Division

Presented at the International Symposium on
Processing of Advanced Ceramics,
Cincinnati, OH, May 1–5, 1988, and
to be published in the Proceedings

Pore Drag in Alumina

J. Rödel and A.M. Glaeser

October 1988

Prepared for the U.S. Department of Energy under Contract Number DE-AC03-76SF00098.

DISCLAIMER

LBL-25225

Pore Drag in Alumina

J. Rödel and A.M. Glaeser

Department of Materials Science and Mineral Engineering
University of California
and
Materials and Chemical Sciences Division
Lawrence Berkeley Laboratory
1 Cyclotron Road
Berkeley, California 94720
USA

October 1988

PORE DRAG IN ALUMINA

J. Rödel and A. M. Glaeser
Department of Materials Science and Mineral Engineering and
Materials and Chemical Sciences Division
Lawrence Berkeley Laboratory
University of California
Berkeley, California 94720

ABSTRACT

A model experiment is introduced that allows the study of pore drag and pore-boundary separation under conditions of constant density. Photolithography, ion beam etching, and hot pressing were used to generate microdesigned interfacial pore arrays, consisting of pores of controlled size and spacing, in alumina. Results from an investigation of pore drag suggest that the surface diffusivity in MgO-doped alumina exceeds that in undoped alumina by a factor of 2 to 9 at 1600°C. The condition for pore-boundary separation was found to depend strongly on pore spacing; the influence zone of pores is several microns wide. Concurrent studies of the grain boundary mobility show that the migration rate of basal plane sapphire into undoped alumina is lower than that into MgO-doped alumina.

INTRODUCTION

Our understanding of sintering, and our ability to interpret sintering data suffer from several difficulties. The geometry of a powder compact (at the particle level) is often poorly defined. Many concurrent, competitive, and interactive processes contribute to what we refer to as "sintering behavior". Minor impurities can significantly affect more than one of the competitive processes (e.g., MgO in alumina),[1] and consequently, the role of dopants is only marginally understood. Finally, although effects of anisotropy are known to be important,[2] sintering models approximate materials as being isotropic.

Significant advances in our understanding of sintering have resulted from modelling sintering as a competition between densification and coarsening processes,[3,4] and investigating the

competitive processes individually. Ideally, hot pressing provides a means of studying densification in the total absence of coarsening. Practically, the pressure-induced acceleration of densification reduces the extent of grain growth, and thus, reduces its effect on densification. Although some coarsening does occur, hot pressing has nonetheless been valuable in helping to identify densification mechanisms,[5] and thus, is one of the experiments needed to systematically investigate the component processes of sintering. Recently, we proposed an experimental technique for studying pore elimination and coarsening,[6] which is based on methods similar to those discussed in this paper, and may provide further insights pertinent to grain boundary transport.

An improved understanding of coarsening processes is also needed. Investigations of (grain) coarsening in a pore-free material are the most straightforward, and have indicated that the grain boundary mobility is significantly lower in MgO-doped alumina than in the undoped material.[7,8] The characteristics of grain growth in porous compacts, specifically the nature of pore-boundary interactions during sintering, also have an important effect on microstructural evolution. The interaction of individual pores with grain boundaries has been modelled by Evans and co-workers.[9-11] In contrast, interactions between arrays of pores and grain boundaries have been modelled at a more fundamental level.[12-14]

Experiments capable of critically testing models of pore-boundary interactions were lacking. As a result, experimental studies of pore drag were limited to one of two approaches. The first is indirect. Since the migration of sufficiently fine pores is controlled by surface transport, some studies have focussed on measuring the surface diffusivity D_s.[2,15] Differing measurement techniques applied to materials with differing impurity contents have yielded a wide range of surface diffusivities for alumina. When higher purity single crystals are used, surface orientation related differences in surface structure or surface energy anisotropy (or both) can affect surface transport rates. In a recent study of pore morphology evolution in sapphire, the pore channel orientation (direction) within a given plane had a significant effect on the behavior.[16]

The alternative approach to studying pore drag yields qualitative information. A comparison and interpretation of the grain size-density plots for MgO-doped and undoped alumina led Berry and Harmer[17] to conclude that the surface diffusivity in alumina is increased by a factor of $\simeq$2.5 by the addition of 250 ppm MgO. Exact values of D_s could not be extracted from the results.

It would be very desirable to have an experimental procedure amenable to controlled study of pore drag, which would allow

determination of the critical condition for pore-grain boundary separation.[18] Ideally, this experiment would circumvent the problems associated with sintering studies, that is, it would provide a well-defined geometry, and it would eliminate competitive densification processes. The experimental procedure presented in this paper satisfies these restrictions, and thus, provides a tool for conducting "controlled pore drag" experiments. Such controlled pore drag experiments, together with hot pressing experiments, allow study of the two idealized or limiting paths of microstructural evolution during sintering, as represented in Figure 1.

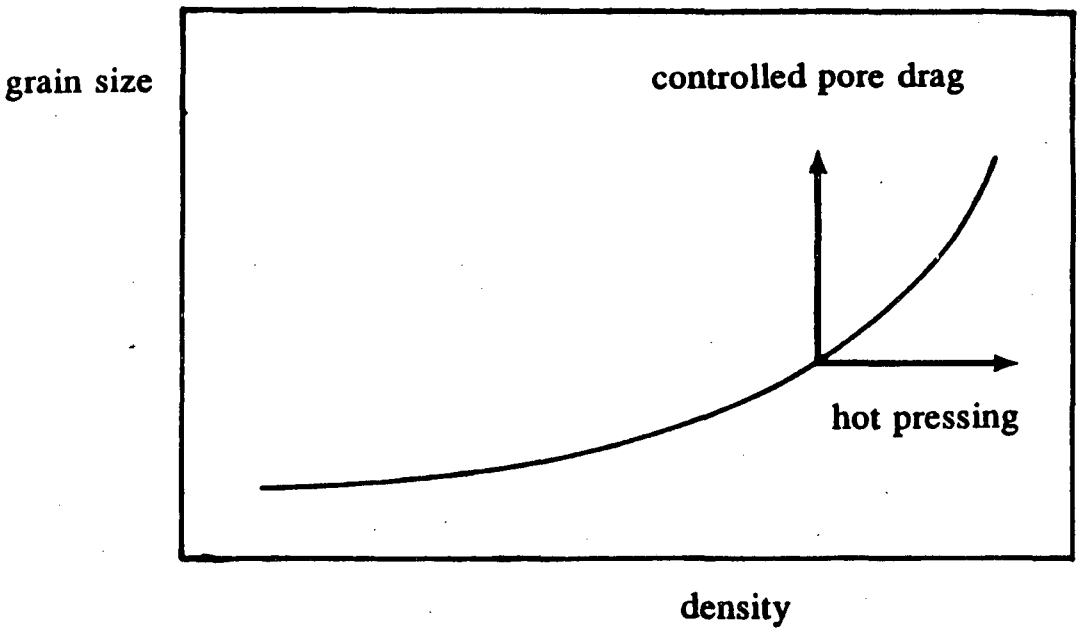

Figure 1 Schematic of sintering trajectory including idealized paths corresponding to hot pressing (zero coarsening) and controlled pore drag (zero densification) experiments.

EXPERIMENTAL METHOD

Sample preparation:

Controlled pore drag experiments rely on the production of controlled-geometry pore structures[19] at the interface between a large grain (single crystal sapphire) and a dense polycrystalline matrix. During subsequent heat treatments, the large "abnormal" grain consumes the adjoining polycrystalline material at a rate determined by the drag force exerted by the interfacial pore

arrays.* Since both pore size and spacing can be precisely controlled and easily varied, a wide range of conditions can be examined.

Controlled surface structures were generated on the basal plane of sapphire by sequential application of photolithographic methods and ion beam etching. Computer-generated data files were used to design a mask, which in turn, was used to selectively expose a photoresist-coated sapphire wafer.** The photoresist was developed, and the sapphire was subsequently etched with an ion beam. Examples of resulting surface structures are shown in Figure 2; the pore width is 3 μm, center-to-center pore spacings are 4, 6, 8, and 10 μm, and the pore depth is 0.24 μm.

A wide range of pore structures was developed at the single crystal-polycrystal interface. Pore arrays 20 pores wide and 1800 to 4000 pores long with interarray spacings of 200 μm were produced. In addition to the pore arrays, wide channels were etched into the sapphire surface. These allowed convenient measurement of the pore depth using a surface profilometer, and also marked the position of the interface prior to migration into the polycrystalline matrix.

Etched sapphire wafers were subsequently hot pressed against highly polished dense polycrystals (Figure 3), thus transferring the controlled pore structures from external to internal interfaces (Figure 4). Wide pore-free ligaments surrounding the pore arrays were used to almost completely suppress densification during hot pressing and annealing.

The theoretically dense polycrystalline aluminas were fabricated using a two-stage hot pressing and hot isostatic pressing procedure. Prolonged exposure to elevated temperature was avoided in order to limit the amount of grain growth and contamination, thus preserving a fine-grained high purity or intentionally doped matrix.

---

*Micrographs from Coble's original experiments, in which single crystal sapphire spheres were used to seed abnormal grain growth, indicate that pores inadvertently generated at the interface were also dragged with the boundary for short distances.

**Adolf Meller Co., Providence RI.

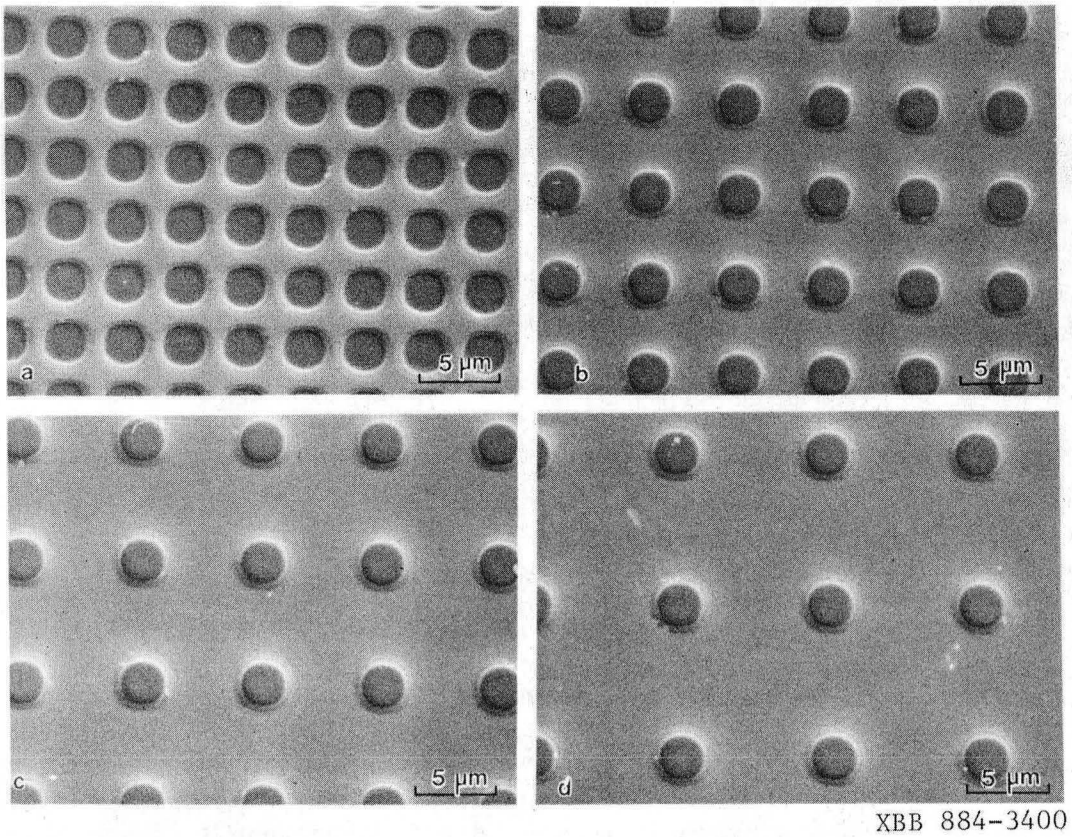

XBB 884-3400

Figure 2 Examples of surface structures used for controlled pore drag experiments. The pore width is 3 μm, center-to-center pore spacings are a) 4 μm, b) 6 μm, c) 8 μm, and d) 10 μm, and the pore depth is 0.24 μm.

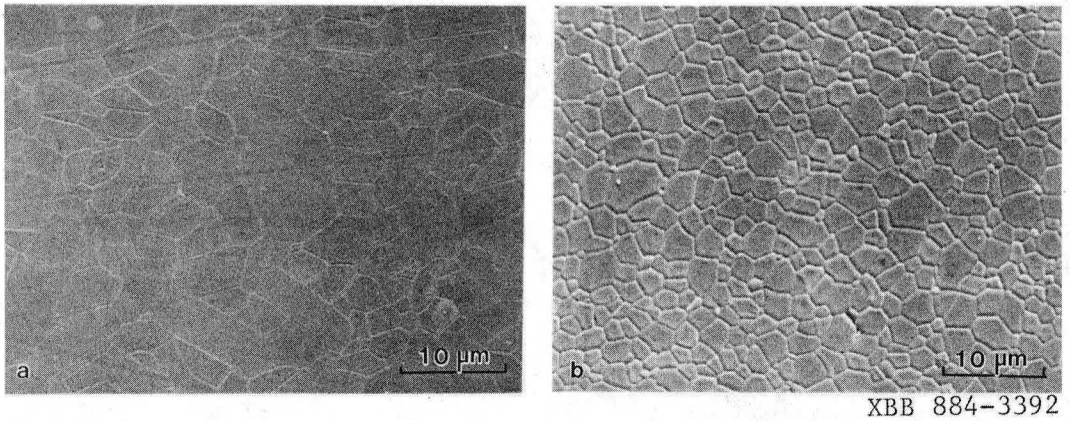

XBB 884-3392

Figure 3 Polycrystalline aluminas obtained by combined hot pressing and hot isostatic pressing; a) undoped alumina, and b) 250 ppm MgO-doped alumina.

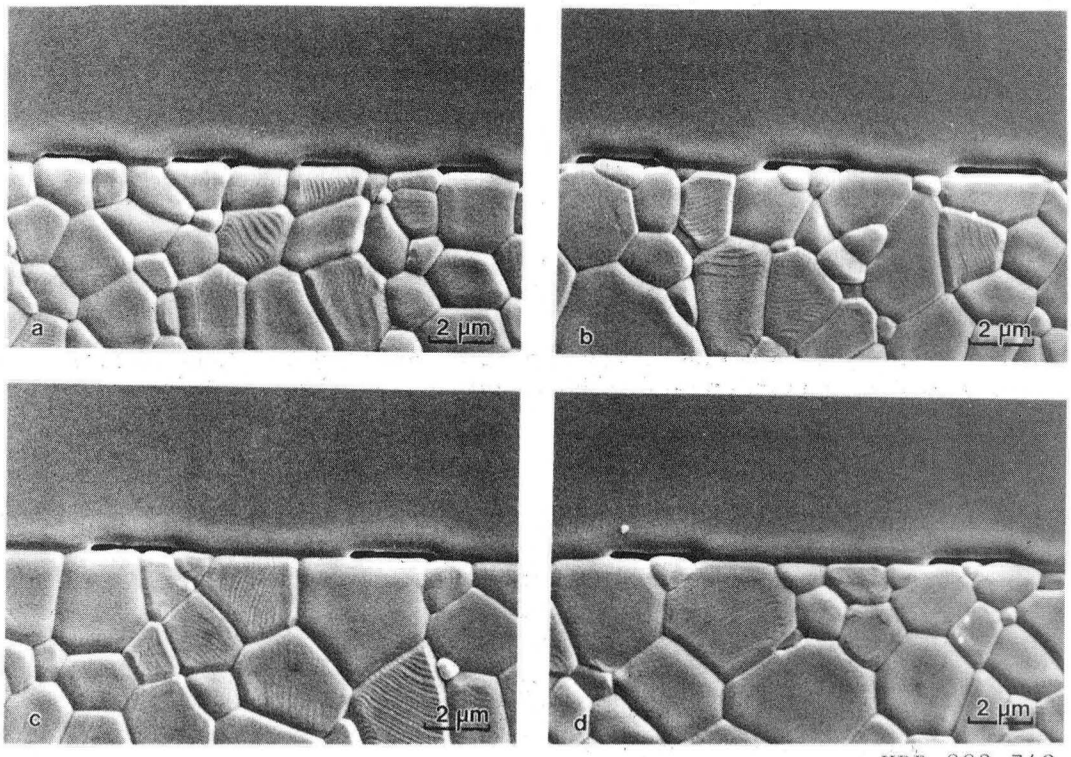

XBB 882-742

Figure 4 Pore structures at the interface between sapphire and MgO-doped alumina. Pore spacings and structures are identical to those in Figure 2.

Undoped alumina* was hot pressed at 1410°C for 2 h under a pressure of 35 MPa, using a boron nitride coated graphite die and boron nitride spacers.** This yielded material with a relative density of 99.4%. Subsequently, hot isostatic pressing at 175 MPa for 1 h at 1500°C was used to complete densification.

The doped material was produced by mixing alumina powder* with sufficient double distilled water-$Mg(NO_3)_2 \cdot 6H_2O$ solution to introduce 250 atomic ppm MgO. Mixing was performed in a Teflon® beaker. The mixed powders were dried at 80°C, and subsequently calcined for 2 h at 600°C. The powder was lightly crushed with a Teflon® rod before loading into the hot pressing die. For this material, hot pressing was performed at 1375°C for 50 min using

---

*Sumitomo, A-HPT-F, New York NY.

**Union Carbide, Cleveland OH, HCM boron nitride powder and HBC boron nitride rod.

35 MPa pressure. This yielded material with a density of 98.4%. Hot isostatic pressing for 1 h at 1500°C at 175 MPa pressure produced theoretically dense material.

The microstructures of both undoped and doped materials were uniform. The average grain sizes were 5.6 μm and 3.1 μm for the undoped and doped alumina, respectively. After hot isostatic pressing, slices were cut from the center of the billet, and polished to a 0.25-μm finish prior to bonding to etched basal plane sapphire wafers. The final hot pressed samples had dimensions of 2 x 9 x 18 mm. Because of the transparency of sapphire, it was possible to resolve the positions of the pore arrays and reference channels by optical microscopy, both after initial sample preparation and after subsequent heat treatments.

Measurements:

Samples with controlled interfacial pore structures were cut into slices, which in turn, were cleaned with organic solvents, embedded in powder of identical composition in a high purity alumina crucible, and heat treated for various times at 1600°C in air. After this step, ≈50 to 100 μm of material was removed, the specimens were polished, thermally etched (1 h at 1400°C for MgO doped alumina, 2 h at 1400°C for undoped alumina), and examined using scanning electron microscopy.

The average grain size, G, was determined using the linear intercept method, with each data point representing measurements of at least 200 grains. Grain boundary migration rates were obtained by measuring boundary positions after various tempering times relative to the initial interface position as marked by the reference channels. The channels essentially served as huge pores which separated from the interface at the onset of motion. The accuracy of the boundary displacement measurements were limited by: 1) the accuracy in determining the original boundary position by interpolation between reference channels, and 2) the accuracy with which final boundary positions could be determined when finite width boundary grooves were present. The error in the original boundary position was found to be <0.2 μm; the error in the final boundary position was ± 0.3 μm. The total displacement uncertainty of ≈0.5 μm was taken into account in analyzing the data.

RESULTS

The results presented focus on pore drag kinetics. The essential parameters in models of pore-boundary interactions are the grain boundary mobility, M_b, the pore mobility, M_p, and the areal density of pores. In our study, the mobilities were assessed by measuring grain boundary and pore velocities under

known driving forces; the areal density of pores is controlled using the procedures previously described.

The grain boundary velocity, V_b, was determined by monitoring the growth of unetched (pore-free) basal plane sapphire wafers into both doped and undoped dense alumina polycrystals. M_b was calculated using the relationship

$$V_b = 2\gamma_b M_b \Omega^{2/3}/G \qquad [1]$$

where γ_b is the grain boundary energy (0.45 J/m^2),[20] and Ω is the atomic volume (2.11 x 10^{-29} m^3). The relationship assumes that the driving force for atomic transport across the boundary is proportional to the pressure difference between the two sides of the boundary. The instantaneous values of the grain boundary mobility (at the point of separation) were calculated by determining the instantaneous grain boundary velocities (by differentiating the time displacement curve) and the corresponding instantaneous average grain sizes (from grain growth data). Results indicate a mobility of 6.2 x 10^{10} μm/Ns for growth into undoped alumina at 1600°C, and a mobility of 7.9 x 10^{10} μm/Ns for the doped material. The higher grain boundary mobility in the doped material contradicts the general trend towards lower mobility (in doped material) inferred from results of previous studies.[7,8] Recent experiments have indicated that grain boundaries oriented parallel to the basal plane in glass-containing alumina have a relatively low mobility, and contribute to the development of anisotropic facetted grain shapes.[21] TEM characterization of the single crystal-polycrystal interface, and experiments using sapphire crystals of differing surface orientation are planned, and should help determine: 1) if a glassy phase is present in our samples, 2) if a glassy phase is absent, whether the dopant changes the interface structure, and 3) if the increased mobility due to MgO-doping is peculiar to the basal plane.

We now address grain boundary migration rates under the influence of pore drag. There are two issues that require discussion. The first deals with the shape changes of the initially "flat" pores prior to their being dragged along by the migrating boundary. The second issue deals with the actual grain boundary migration rates of interfaces with controlled geometry pore arrays and the condition for pore-boundary separation.

The first issue is specific to our method of specimen preparation. The pores initially have a width-to-depth ratio >10, and are far from an equilibrium shape. However, this has its advantages, in that the high effective areal fraction of pores inhibits premature pore-boundary separation, and thus allows pore equilibration to occur. As the pore shapes become more nearly equilibrated, migration of the pore-boundary ensemble

initiates. Figure 5 illustrates a pore array in undoped alumina after (a) 10 h and (b) 20 h heat treatments at 1600°C.* Pores in MgO-doped alumina develop more equiaxed shapes in shorter times than in undoped alumina.

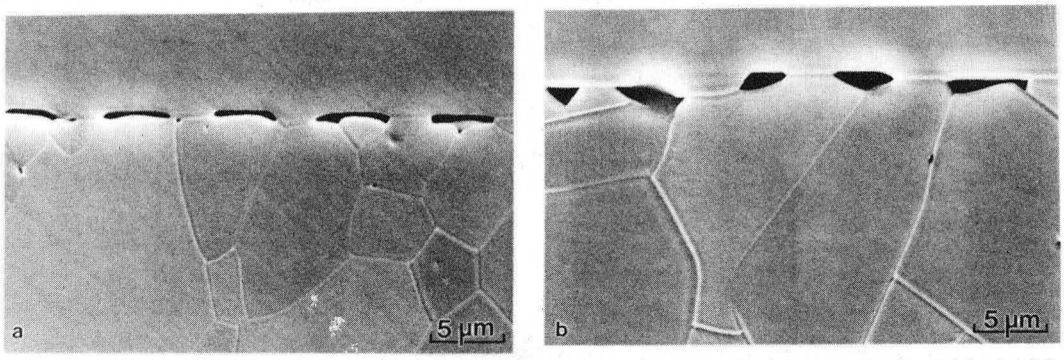

XBB 884-3498

Figure 5 Morphological evolution of initially flat pores in alumina after a) 10 h, and b) 20 h at 1600°C.

Pore-boundary attachment is illustrated for MgO-doped alumina in Figure 6, whereas pore-boundary separation is illustrated in Figure 7. Grain boundary migration rates under pore attachment conditions for undoped and doped alumina are presented in Figures 8a and 8b, respectively. Pores at the undoped alumina-sapphire interface were initially immobile. Subsequently (after some equilibration), pores with small interpore spacings were dragged along for a short distance without separation. The total extent of motion was limited because concurrent matrix grain growth significantly reduced the driving force for further migration of the pore-laden alumina-sapphire interface. Arrays of pores in the undoped alumina with larger interpore spacing were dragged along for ≈2 μm, versus an ≈8 μm displacement for the pore-free grain boundary in the same time, and then separated from the sapphire-alumina interface. Pore arrays in the MgO-doped alumina remained attached and migrated at a constant rate for 10 h, and then separated. After 10 h at 1600°C, the displacement of the pore-laden boundary was ≈6 μm, versus ≈13 μm for the pore-free

---

*This figure illustrates a rather extreme case involving pores initially 5.0 μm wide and 0.25 μm deep, with an initial spacing of 8.0 μm. After 10 h, migration had just initiated; after 20 h, the migration rate is sufficiently low that pores appear to be facetting.

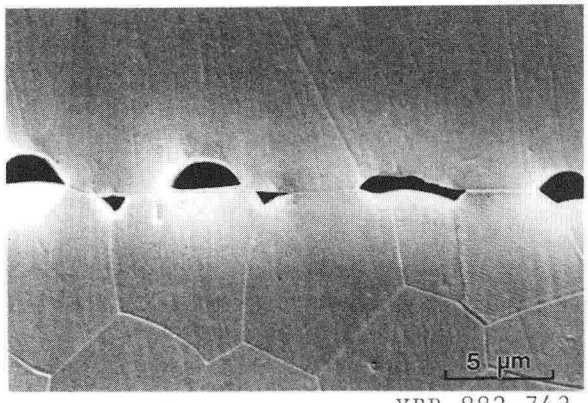

Figure 6 Illustration of pore drag in MgO-doped alumina.

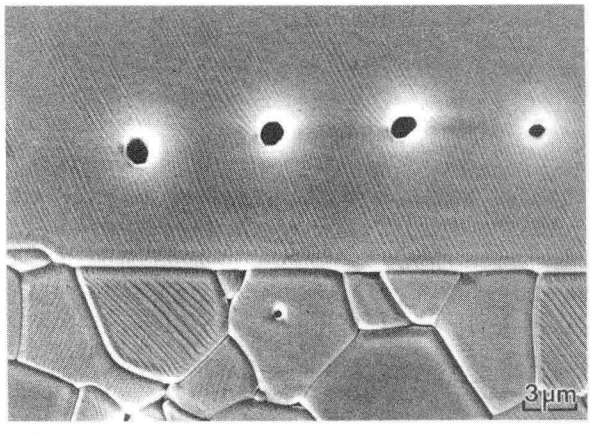

Figure 7 Example of pore-boundary separation in MgO-doped alumina. XBB 884-3500

boundary. Figure 9 illustrates separated pore arrays in MgO-doped alumina with two different spacings; samples were annealed 15 h at 1600°C. We emphasize that all the data points presented were derived from the behavior of arrays of pores, rather than from the behavior of individual pores.

DISCUSSION

Our results include measurements of the pore velocities just prior to pore-boundary separation, and therefore velocities approaching the peak pore velocity. When measurement errors are taken into account, the peak pore velocity, V_p, for undoped alumina is in the range of 0.08 to 0.22 μm/h, whereas the range for MgO-doped alumina is between 0.45 to 0.70 μm/h. Hsueh, Evans and Coble calculated steady-state pore shapes as a function of

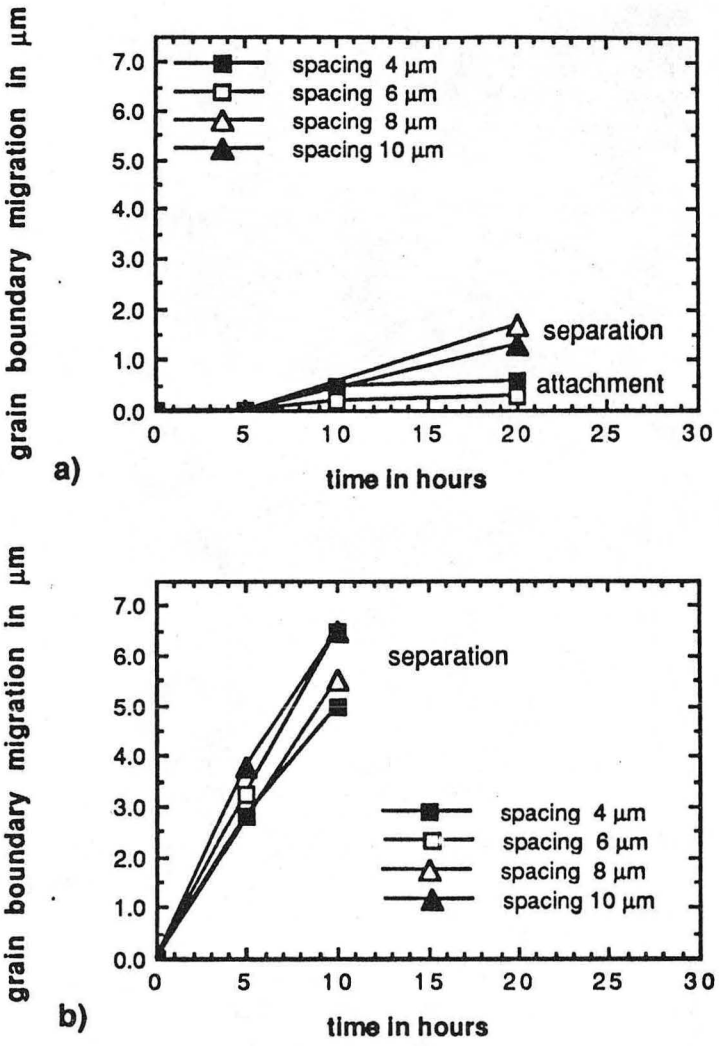

Figure 8 Grain boundary migration versus time at 1600°C for various pore spacings; a) undoped alumina, and b) MgO-doped alumina.

pore velocity, and derived a relationship between V_p (the velocity near separation) and the surface diffusivity, ^pD_s,[9]

$$V_p \simeq [\Omega D_s \delta_s \gamma_s / kTr^3] \cdot (17.9 - 6.2\psi) \qquad [2]$$

where γ_s is the specific surface energy, δ_s the diffusion width, r the radius of a spherical pore of equivalent volume (0.67 μm in our case), and ψ is the dihedral angle in radians. For the present purposes, we have used reported averages for γ_s (0.9 J/m^2)[20] and ψ (≃115° for undoped alumina, and 117° for MgO-doped

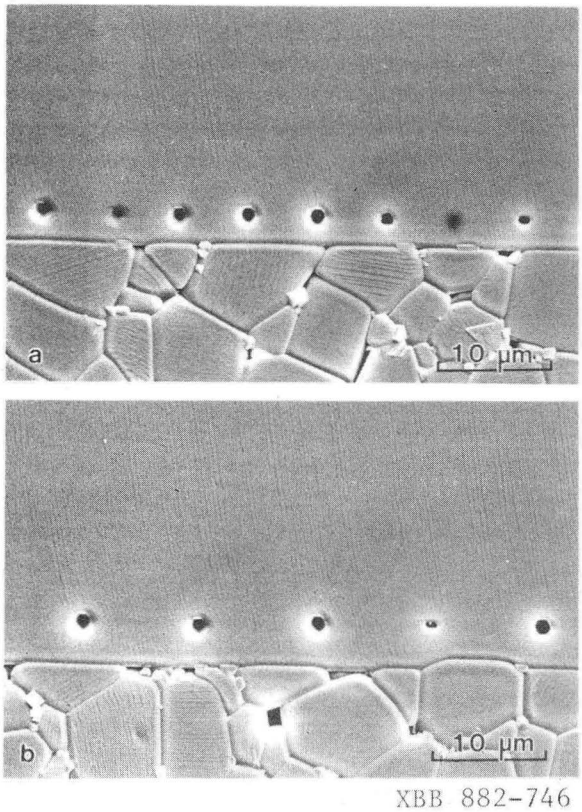

XBB 882-746

Figure 9 Pore-boundary separation in MgO-doped alumina at two different pore spacings. The sample was annealed for 15 h at 1600°C. Separation occurred after ≈10 h.

alumina).[22] Substituting these values into Eq. 2 yields D_s = 0.55-1.51 x 10^{-7} cm^2/s for the undoped alumina, and D_s = 3.24-5.04 x 10^{-7} cm^2/s for the MgO-doped alumina. This suggests that the addition of 250 ppm MgO increases the surface diffusivity by a factor of 2 to 9 at 1600°C.

Calculation of separation conditions entails substitution of the measured peak pore velocities, expressed in the form of Eq. 2, into an expression describing pore-boundary separation in the case of constant center-to-center pore spacing, f.[14] The appropriate expression is:

$$G^{-1} = [\delta_s \Omega^{1/3} D_s \gamma_s \cdot (17.9 - 6.2\psi)/2kTM_b \gamma_b r^3] + \pi r/f^2 \qquad [3]$$

This relationship allows us to divide grain size-pore size maps into regions in which either pore separation or pore attachment are expected. The ratio of critical coefficients such as D_s and M_b can be measured from the same experiment. The actual and

predicted critical conditions for pore-boundary separation can be compared, thus allowing a check of the original results. Two sources of error will affect the closeness of the agreement. The uncertainty in V_p, or equivalently the uncertainty in D_s in Eq. 3, defines a separation area rather than a separation line. In addition, there is some uncertainty in the exact grain size when separation occurred, due to matrix grain growth.

The correspondence between calculated pore-boundary separation conditions and observed behavior is illustrated in Figures 10a and 10b for undoped and MgO-doped alumina, respectively. The points plotted again represent or characterize the behavior of entire pore arrays, not isolated pores. Given the uncertainties in the values of the interfacial energies, the dihedral angles, and the grain boundary mobility, the agreement between calculated and observed pore-boundary separation conditions is encouraging. For undoped alumina, the correlation is particularly good. The effect of pore spacing is noteworthy. Hsueh et al. compared V_p with the boundary velocity outside the pore's zone of influence, and thus developed a separation criterion independent of pore spacing, i.e., like Eq. 3 with $f = \infty$.[9] Our experiments demonstrate that the influence zone is several microns wide, and thus, the velocity of the pore-laden boundary must be considered for comparison. For MgO-doped alumina, two data points fall into the region of experimental uncertainty, while two pore arrays show separation as predicted. Further experiments using a coarser grain size matrix are necessary to define the transition condition.

Finally, a few comments pertaining to the MgO concentration at the single crystal-polycrystal interface seem appropriate. Initially, there is a discontinuous change in the MgO concentration at the single crystal-polycrystal interface, from nearly 0 to ≈250 ppm. Interdiffusion will reduce the MgO content of the adjoining polycrystalline matrix. In our case, migration of the interface into the doped matrix will at least partially offset this localized depletion of dopant concentration. Furthermore, we anticipate that grain boundary diffusion of the dopant on the polycrystalline side of the interface will tend to reduce concentration gradients in the doped material. As a result, we expect the bulk concentration of MgO in the polycrystalline matrix to lie between 125 and 250 ppm.

SUMMARY

It is possible to study the kinetics of pore drag and to assess the conditions for pore-boundary separation using the method of controlled pore drag. The method's viability has been demonstrated using alumina, but the technique can be applied to a wide range of materials. Since this model experiment closely

simulates pore-boundary interactions during sintering, we anticipate that the information derived will be more directly applicable to modelling microstructural evolution than results obtained from surface diffusion experiments using single crystals. Further work is needed to define the pore separation and attachment regions, and the kinetics of pore drag in alumina more accurately.

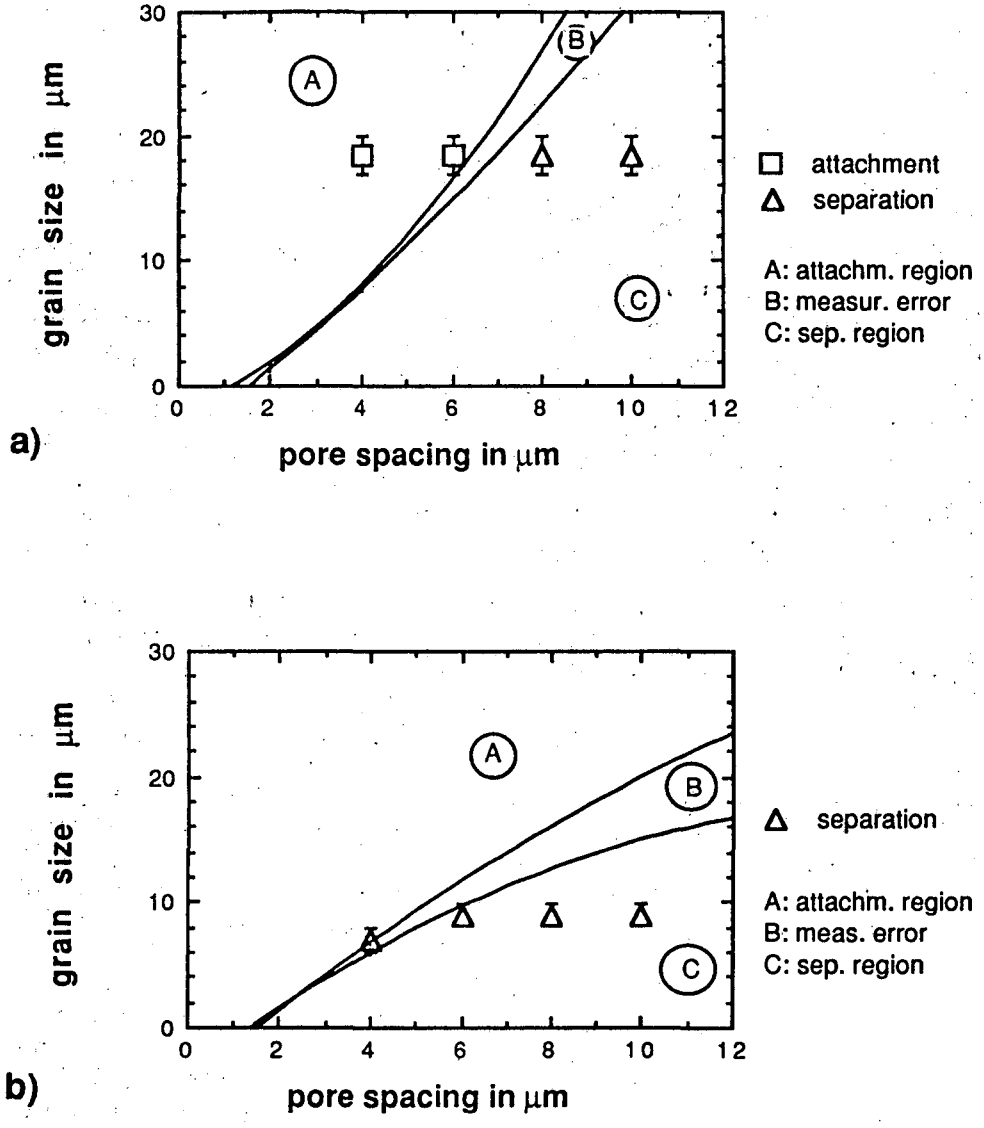

Figure 10 Calculated and observed separation conditions for a) undoped, and b) doped alumina.

Acknowledgements:

This work was supported by the Director, the Office of Energy Research, Office of Basic Energy Sciences, Materials Sciences Division of the U. S. Department of Energy under Contract No. DE-AC03-76SF00098. The microfabrication processing was performed at the Microfabrication Laboratory in the Department of Electrical Engineering and Computer Science at the University of California, Berkeley; we thank the staff for their assistance.

References:

1. R. L. Coble, "Sintering Crystalline Solids. II. Experimental Test of Diffusion Models in Powder Compacts," J. Appl. Phys., 32, [5], 793-99 (1961).
2. J. Rödel and A. M. Glaeser, "Morphological Evolution of Pore Channels in Alumina," these Proceedings.
3. C. A. Handwerker, R. M. Cannon and R. L. Coble, "Final Stage Sintering of MgO," Advances in Ceramics, Vol. 10, edited by W. D. Kingery, pp. 619-643 (1984).
4. M. F. Yan, "Microstructural Control in the Processing of Electronic Ceramics," Mat. Sci. and Eng., 48, [1], 53-72 (1981).
5. M. P. Harmer and R. J. Brook, "The Effect of MgO Additions of the Kinetics of Hot Pressing in Al_2O_3," J. Mater. Sci., 15, [12], 3017-24 (1980).
6. J. Rödel and A. M. Glaeser, "A Technique for Investigating The Elimination and Coarsening of Model Pore Arrays," Materials Letters, 6, [10], 351-55, (1988).
7. S. J. Bennison and M. P. Harmer, "Effect of MgO Solute on the Kinetics of Grain Growth in Al_2O_3," J. Am. Ceram. Soc., 66, [5], C90-C92 (1983).
8. S. J. Bennison and M. P. Harmer, "Grain Growth Kinetics for Alumina in the Absence of a Liquid Phase," J. Am. Ceram. Soc., 68, [1], C22-C24 (1985).
9. C. H. Hsueh, A. G. Evans, and R. L. Coble, "Microstructure Development During Final/Intermediate Stage Sintering - I. Pore/Grain Boundary Separation," Acta Metall., 30, [7], 1269-79 (1982).
10. M. A. Spears and A. G. Evans, "Microstructure Development during Final/Intermediate Stage Sintering - II. Grain and Pore Coarsening," Acta Metall., 30, [7], 1281-89 (1982).
11. C. H. Hsueh and A. G. Evans, Microstructure Evolution during Sintering: The Role of Evaporation/Condensation," Acta Metall., 31, [1], 189-98 (1983).
12. R. J. Brook, "Pore-Grain Boundary Interactions and Grain Growth," J. Am. Ceram. Soc., 52, [1], 56-57 (1969).

13. R. J. Brook, "Controlled Grain Growth"; pp. 331-64 in Treatise on Materials Science and Technology, Vol. 9, Edited by F. F. Y. Wang, Academic Press, New York, 1976.
14. F. M. A. Carpay, "Discontinuous Grain Growth and Pore Drag," J. Am. Ceram. Soc., 60, [1-2], 82-83 (1977).
15. T. K. Gupta, "Instability of Cylindrical Voids in Alumina," J. Am. Ceram. Soc., 61, [5-6], 191-95 (1978).
16. F. H. Huang, R. A. Henrichsen and Che-Yu Li, "A Study of Capillarity and Mass Transport on the Al_2O_3 Surface," Mat. Sci. Res., 10, 173-86 (1975).
17. K. A. Berry and M. P. Harmer, "Effect of MgO Solute on Microstructure Development in Al_2O_3," J. Am. Ceram. Soc., 69, [2], 143-49 (1986).
18. M. P. Harmer, "Use of Solid-Solution Additives in Ceramic Processing," pp. 679-98 in Advances in Ceramics, Vol. 10, Edited by W. D. Kingery (1984).
19. J. Rödel and A. M. Glaeser, "Production of Controlled Morphology Intergranular Pore Arrays: Implications and Opportunities," J. Am. Ceram. Soc., 70, [8], C172-C175 (1987).
20. W. D. Kingery, "Metal-Ceramic Interactions: IV, Absolute Measurement of Metal-Ceramic Interfacial Energy and the Interfacial Adsorption of Silicon for Iron-Silicon Alloys," J. Am. Ceram. Soc., 37, [2], 42-45 (1954).
21. W. A. Kaysser, M. Sprissler, C. A. Handwerker, and J. E. Blendell, "Effect of Liquid Phase on the Morphology of Grain Growth in Alumina," J. Am. Ceram. Soc., 70, [5], 339-43 (1987).
22. J. E. Blendell and C. A. Handwerker, "Effect of Chemical Composition on Sintering of Ceramics," J. Cryst. Growth, 75, [1], 138-60 (1986).

LAWRENCE BERKELEY LABORATORY
TECHNICAL INFORMATION DEPARTMENT
UNIVERSITY OF CALIFORNIA
BERKELEY, CALIFORNIA 94720